This is a repository copy of *Stability analysis and nonlinear current-limiting control design for DC micro-grids with CPLs*.

White Rose Research Online URL for this paper:
http://eprints.whiterose.ac.uk/157775/

Version: Published Version

Article:
Braitor, A.-C. orcid.org/0000-0002-7666-0457, Konstantopoulos, G. and Kadirkamanathan, V. (2020) Stability analysis and nonlinear current-limiting control design for DC micro-grids with CPLs. IET Smart Grid, 3 (3). pp. 355-366. ISSN 2515-2947

https://doi.org/10.1049/iet-stg.2019.0235

Reuse
This article is distributed under the terms of the Creative Commons Attribution (CC BY) licence. This licence allows you to distribute, remix, tweak, and build upon the work, even commercially, as long as you credit the authors for the original work. More information and the full terms of the licence here: https://creativecommons.org/licenses/

Takedown
If you consider content in White Rose Research Online to be in breach of UK law, please notify us by emailing eprints@whiterose.ac.uk including the URL of the record and the reason for the withdrawal request.

eprints@whiterose.ac.uk
https://eprints.whiterose.ac.uk/

IET Smart Grid

Research Article

IET Journals
The Institution of Engineering and Technology

Stability analysis and nonlinear current-limiting control design for DC micro-grids with CPLs

eISSN 2515-2947
Received on 2nd September 2019
Revised 12th December 2019
Accepted on 25th February 2020
E-First on 21st May 2020
doi: 10.1049/iet-stg.2019.0235
www.ietdl.org

Andrei-Constantin Braitor[1] ✉, *George C. Konstantopoulos*[1], *Visakan Kadirkamanathan*[1]

[1]*Department of Automatic Control and Systems Engineering, The University of Sheffield, Sheffield, S1 3JD, UK*

✉ *E-mail: abraitor1@sheffield.ac.uk*

Abstract: In this study, a DC micro-grid consisting of multiple paralleled energy resources interfaced by both bidirectional AC/DC and DC/DC boost converters and loaded by a constant power load (CPL) is investigated. By considering the generic *dq* transformation of the AC/DC converters' dynamics and the accurate nonlinear model of the DC/DC converters, two novel control schemes are presented for each converter-interfaced unit to guarantee load voltage regulation, power sharing and closed-loop system stability. This novel framework incorporates the widely adopted droop control and using input-to-state stability theory, it is proven that each converter guarantees a desired current limitation without the need for cascaded control and saturation blocks. Sufficient conditions to ensure closed-loop system stability are analytically obtained and tested for different operation scenarios. The system stability is further analysed from a graphical perspective, providing valuable insights of the CPL's influence onto the system performance and stability. The proposed control performance and the theoretical analysis are first validated by simulating a three-phase AC/DC converter in parallel with a bidirectional DC/DC boost converter feeding a CPL in comparison with the cascaded PI control technique. Finally, experimental results are also provided to demonstrate the effectiveness of the proposed control approach on a real testbed.

1 Introduction

Driven by the energy crisis, environmental pollution and greenhouse gas emissions [1–3], the seamless integration of renewable energy sources (RESs) has been actively pursued worldwide, over the past decades. With the uninterrupted growth of RES, the smart grid and micro-grid concepts have been proposed as a benchmark of the future grid to enable efficient utilisation of renewable resources and distributed generations (DGs). The centrepiece of these frameworks is represented by the power converters [4] which are the interface devices of RES to the micro-grid system.

In DC micro-grids, DG units are connected to a common DC bus through AC/DC and/or DC/DC converters, often operating in parallel leading to a series of non-trivial issues such as voltage regulation and accurate distribution of the load power. A widely used technique to accomplish these tasks, implemented in a fully decentralised way, that does not require communication between each DG, is to introduce a virtual resistance at the output of each converter, a method also referred to as 'droop control' [5–9]. The main disadvantages of the conventional droop control consist of significant load voltage drop and inaccurate power sharing due to mismatches at the line impedances. Therefore, several methods have been proposed to tackle and improve its existing performance, such as the robust droop control [10, 11] where the line impedances are not considered, the nonlinear droop control [12] where each DG unit is optimised against hypothetical DGs, or the quadratic droop control [13], implemented as a special case of the general feedback controller. However, in the majority of these works, the stability of the parallel operated power converters has been insufficiently addressed mainly due to the complexity of the dynamics that increases with the nonlinear characteristics of the AC/DC and DC/DC converters and their nonlinear loads. Power converters fed by the main bus create unique dynamic characteristics and have been a research subject for years. As shown in [14, 15], under tight-speed regulation, the motor drive exhibits constant power behaviour at the DC bus, similar to tight regulated downstream converters [16–18]. The dynamic behaviour of constant power loads is equivalent to a dynamic negative impedance which can produce instability at the DC bus and, consequently, in the system [16]. Limitations of practical constant power loads (CPLs) in real-world applications have been assessed in [17], and there is an increased interest in designing droop controllers that guarantee closed-loop system stability for DC micro-grids loaded by CPLs [19, 20].

The existing stability methods for investigating DC micro-grids are based on the small-signal model of the power devices and linear approximation approaches, mostly employing the Middlebrook and Cuk criterion [21]. Whilst small-signal modelling is useful to obtain the system's open-loop gain by considering only the input impedance of the loads and output impedance of the sources [22, 23], the nonlinear dynamics of the power converters are not taken into account. Stability of reduced-order models has been investigated in [24, 25] and stable operating regions have been obtained, but they ignore the dynamic performances of the DC-DC converters. Global stability results can be obtained using nonlinear control techniques, such as passivity-based control (PBC) methods, which have been successfully applied to power converter systems applications [26, 27]. However, these control schemes require the knowledge of the system and load parameters, which may not be available in practice. To overcome this issue, advanced control techniques such as adaptive PBC [28] or the interconnection and damping assignment PBC (IDA-PBC) [29] have been designed. Particularly, the IDA-PBC guarantees closed-loop stability with enhanced system robustness as it is parameter free. However, its main shortcoming is that it needs the solution of a partial differential equation (PDE) system of order equal to the system order. Thus, in a DC micro-grid application with multiple DC/DC and AC/DC converters, the PDE solution cannot be analytically obtained.

Apart from achieving stability in the micro-grid, other control issues that relate to the technical requirements of each DG unit should be taken into account in the control design such as the capability of the power converters to be protected at all times, particularly during transients, faults and unrealistic power demands. The overcurrent protection as presented in [30, 31], guarantees the converter operation and protection of the equipment without violating its technical limitations. Existing strategies are based on protection units such as using additional fuses, circuit breakers or relays [32–34]; however, it still represents a challenge

This is an open access article published by the IET under the Creative Commons Attribution License (http://creativecommons.org/licenses/by/3.0/)

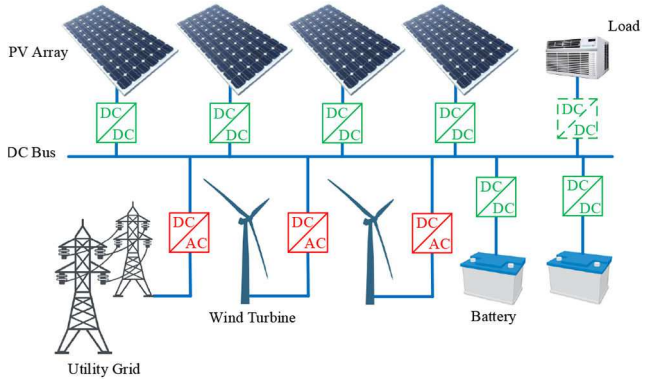

Fig. 1 *Typical configuration of a DC micro-grid*

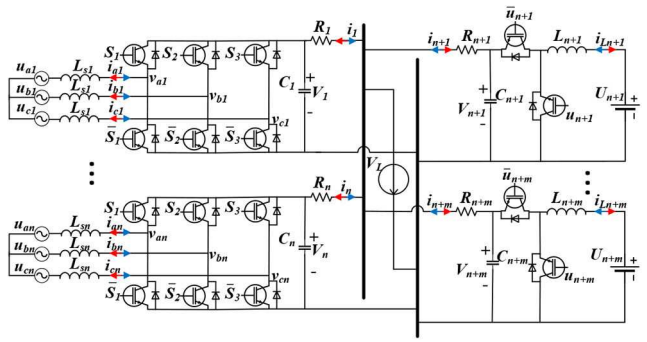

Fig. 2 *Parallel operated three-phase AC/DC and bidirectional DC/DC boost converters feeding a common constant power load*

to design control methods that ensure an inherent current-limiting property [35–37]. Although current-limiting control methods based on saturated *PI* controllers are often used to guarantee a given upper limit for the current, the shortcomings of these methods have not been completely overcome, e.g.: (i) only the reference value of the converter's input current is limited, i.e. overcurrent protection is not achieved during transients as shown in [31] and (ii) closed-loop stability cannot be analytically guaranteed since the controller can suffer from integrator wind-up problems that could potentially yield instability in the system [38].

For this reason, in this paper, two novel nonlinear droop control strategies are proposed for parallel operated bidirectional three-phase AC/DC and DC/DC boost converters feeding a CPL in a DC micro-grid architecture to ensure accurate distribution of the load power among the paralleled units in proportion to their power ratings and inherent overcurrent protection. Based on the nonlinear dynamics of the converters and using input-to-state stability (ISS) theory, it is proven that the proposed controllers guarantee an inherent current-limiting property for each converter independently from each other or the load. In addition, accurate power sharing and load voltage regulation close to the rated value are accomplished and the stability of the closed-loop system is proven when connected to a CPL using singular perturbation theory. The effectiveness of the proposed controllers and the stability conditions are verified through simulation testing and they are compared to the cascaded *PI* technique to highlight its superiority.

One distinctive fact is that compared to the cascaded *PI* approach or when a linear resistive load has been used [31, 39, 40], in this paper a new control structure is proposed that does not require the measurement of the converter output currents and additionally guarantees closed-loop system stability with a CPL. Moreover, in contrast to the control methods and stability analysis of the DC micro-grid presented in [20], the proposed approach not only guarantees stability but also has a better performance in achieving its control tasks whilst ensuring overcurrent protection at all times. The novel contributions of the proposed work are highlighted by the following aspects:

(i) the parallel operation of both bidirectional three-phase AC/DC and DC/DC boost converters is investigated here, which are inherently nonlinear systems, opposed to only unidirectional boost converter [31], or only buck converters, as studied in [20] which have linear dynamics;
(ii) compared to [20], a new droop control structure that achieves improved power sharing and output voltage regulation closer to the rated value is proposed and analysed;
(iii) an inherent current limitation is introduced via the proposed control design for all power converters;
(iv) in contrast to [40] where a linear resistive load was considered, in this paper closed-loop stability is analytically guaranteed for the CPL case.

Therefore, proving closed-loop system stability of a DC micro-grid with a CPL using the nonlinear model of the bidirectional three-phase AC/DC and the DC/DC boost converters together, while guaranteeing improved power sharing accuracy, load voltage regulation and an inherent current-limiting property is to the best of our knowledge novel.

The structure of this paper is divided as follows. In Section 2 the nonlinear model of a DC micro-grid consisting of multiple paralleled bidirectional three-phase AC/DC and DC/DC boost converters is presented. The control framework of the current-limiting droop controller is explained and analysed in Section 3. In Section 4, the closed-loop system stability analysis is presented and then analysed from a graphical perspective in Section 5. In Section 6, simulation results are displayed to test the controller performance, which is further validated in Section 7 on a real experimental testbed. Finally, in Section 8 some conclusions are drawn.

2 Nonlinear model of the DC micro-grid

2.1 Notation

Let $[\boldsymbol{x}] \in \mathbb{R}^{n\times n}$ be defined as the diagonal matrix whose diagonal entries are the elements of the n-dimensional vector $\boldsymbol{x} = [x_1 \ldots x_n]$. Let $\mathbb{O}_n \in \mathbb{R}^n$ and $\mathbb{O}_{n\times n} \in \mathbb{R}^{n\times n}$ be the n-dimensional vector and $n \times n$ square matrix, respectively, with all elements zero, $\boldsymbol{I}_n$ be the identity matrix and let $1_n \in \mathbb{R}^n$ and $1_{n\times n} \in \mathbb{R}^{n\times n}$ be the n-dimensional vector and $n \times n$ square matrix, respectively, with all elements equal to one.

2.2 Dynamic model

A typical topology of a DC micro-grid is shown in Fig. 1 consisting of several types of energy sources, power converters and loads connected to a common bus. The configuration of the DC micro-grid under investigation is shown in Fig. 2, containing n bidirectional three-phase rectifiers and m bidirectional DC/DC boost converters feeding a constant power load, where L_{si} is the inductor at the input, a DC output capacitor C_i with a line resistance R_i and six controllable switching elements that operate using PWM and capable of conducting current and power in both directions. The input voltages and currents of the rectifier are expressed as v_{ai}, v_{bi}, v_{ci} and i_{ai}, i_{bi}, i_{ci}, while output dc voltage is denoted as V_i with $i \in \{1, 2, \ldots, n\}$. The bidirectional DC/DC converters have two switching elements, an inductor L_j at the input and a capacitor C_j with a line resistance R_j at the output, while V_j is the output voltage, where $j \in \{n+1, n+2, \ldots, n+m\}$. At the input, the voltage and the current of the converter are represented as U_j, and i_{Lj}, respectively, with the latter being either positive or negative to allow a bidirectional power-flow.

To obtain the dynamic model of the rectifier, the average system analysis and the dq transformation can be used for three-phase voltages and currents, using Clarke and Park transformations [39]. Following [41], the mathematical model of the rectifiers in the dq coordinates is set up, in matrix form as

$$L_s \dot{I}_d = -\omega L_s I_q - \frac{1}{2} m_d V_r + U_d \tag{1}$$

This is an open access article published by the IET under the Creative Commons Attribution License (http://creativecommons.org/licenses/by/3.0/)

$$L_s\dot{I}_q = \omega L_s I_d - \frac{1}{2}m_q V_{\mathrm{r}} \tag{2}$$

$$C\dot{V}_{\mathrm{r}} = \frac{3}{4}m_d I_d + \frac{3}{4}m_q I_q - i_{\mathrm{r}} \tag{3}$$

where $i_{\mathrm{r}} = [i_1 \dots i_n]^{\mathrm{T}}$, $V_{\mathrm{r}} = [V_1 \dots V_n]^{\mathrm{T}}$, $L_s = \mathrm{diag}\{L_{si}\}$, $C_{\mathrm{r}} = \mathrm{diag}\{C_i\}$, $\omega = \mathrm{diag}\{\omega_i\}$ is the rotating speed, $U_d = [U_{d1} \dots U_{dn}]^{\mathrm{T}}$ is the amplitude of the three-phase AC voltage source when voltage orientation on the d axis is considered and $I_d = [I_{d1} \dots I_{dn}]^{\mathrm{T}}$, $I_q = [I_{q1} \dots I_{qn}]^{\mathrm{T}}$ are the d and q components of the AC source currents, respectively, and $m_d = \mathrm{diag}\{m_{di}\}$, $m_q = \mathrm{diag}\{m_{qi}\}$ are the duty-ratio control inputs of the rectifier with V_d and V_q being the d and q components of the rectifier voltage $v = [v_a\, v_b\, v_c]$, respectively.

Using Kirchhoff laws and average analysis [42], the dynamic model, in matrix form, of the bidirectional DC/DC boost converter becomes

$$L\dot{i}_L = U_b - (\boldsymbol{I}_m - u)V_b \tag{4}$$

$$C_b\dot{V}_b = (\boldsymbol{I}_m - u)i_L - i_b \tag{5}$$

where $i_L = [i_{L(n+1)} \dots i_{L(n+m)}]^{\mathrm{T}}$, $V_b = [V_{n+1} \dots V_{n+m}]^{\mathrm{T}}$, $i_b = [i_{n+1} \dots i_{n+m}]^{\mathrm{T}}$, $U_b = [U_{n+1} \dots U_{n+m}]^{\mathrm{T}}$, $L = \mathrm{diag}\{L_j\}$, $C_b = \mathrm{diag}\{C_j\}$, $u = \mathrm{diag}\{u_j\}$. One can observe that system (1)–(3), (4)–(5) is nonlinear, since the control inputs m_{di}, m_{qi} and u_j are multiplied with the system states, $(I_d, I_q, V_{\mathrm{r}})$, and (i_L, V_b) respectively.

As the AC/DC and DC/DC converters supply a CPL, the power balance equation becomes

$$P = V_L \sum_{k=1}^{n+m} i_k, \tag{6}$$

$$i_k = \frac{V_k - V_L}{R_k} \tag{7}$$

where V_k, i_k represent the output voltages and currents, respectively, with $k \in \{1, 2, \dots, n+m\}$, V_L is the load voltage, and P is constant and represents the power of the CPL. Consider now the following assumptions:

Assumption 1: It holds that

$$\left(\sum_{k=1}^{n+m} \frac{V_k}{R_k}\right)^2 > 4P \sum_{k=1}^{n+m} \frac{1}{R_k}. \tag{8}$$

Thus, substituting the output current i_k from (7) into (6), one can obtain the following expression for the load voltage given by the real solutions of the second order polynomial as

$$V_L = \frac{\sum_{k=1}^{n+m} V_k/R_k \pm \sqrt{\left(\sum_{k=1}^{n+m} V_k/R_k\right)^2 - 4P\sum_{k=1}^{n+m} 1/R_k}}{2\sum_{k=1}^{n+m} 1/R_k}. \tag{9}$$

Assumption 2: Let $I_k^{\max} = \{I_{\mathrm{rms}1}^{\max}, \dots, I_{\mathrm{rms}n}^{\max}, i_{L(n+1)}^{\max}, \dots, i_{L(n+m)}^{\max}\}$ be the maximum input current of each converter (maximum RMS current for AC/DC converters and maximum inductor current for DC/DC converters). Since for three-phase rectifiers $V_i \geq 2U_{di}$ and for boost converters $V_j \geq U_j$, let

$$\min\{2U_{di}, U_j\} - I_k^{\max}R_k > \frac{\sum_{k=1}^{n+m} V_k/R_k \pm \sqrt{\left(\sum_{k=1}^{n+m} V_k/R_k\right)^2 - 4P\sum_{k=1}^{n+m} 1/R_k}}{2\sum_{k=1}^{n+m} 1/R_k}$$

hold, for every $k \in \{1, 2, \dots, n+m\}$.

The load voltage has two solutions, a high voltage and a low voltage, with the high voltage representing the feasible solution because of Assumption 2, which gives $V_L \geq \min\{2U_{di}, U_j\} - I_k^{\max}R_k$. Therefore, the voltage of the load can be described as

$$V_L = \frac{\sum_{k=1}^{n+m} V_k/R_k + \sqrt{\left(\sum_{k=1}^{n+m} V_k/R_k\right)^2 - 4P\sum_{k=1}^{n+m} 1/R_k}}{2\sum_{k=1}^{n+m} 1/R_k}$$

Considering an equilibrium point $(I_{die}, I_{qie}, i_{Lje}, V_{ie}, V_{je})$ for constant control inputs m_{di}, m_{qi}, u_j, by taking the partial derivative of the output current i_k from (7) with respect to the capacitor voltage V_k, we obtain the admittance matrix (see (10)) , where $\boldsymbol{R} = \mathrm{diag}\{R_k\}$ and $\boldsymbol{D} = \mathrm{diag}\{\partial V_L/\partial V_k\}$ with the following expression (see (11)) , where $\sqrt{\left(\sum_{k=1}^{n+m} V_k/R_k\right)^2 - 4P\sum_{k=1}^{n+m} 1/R_k} > 0$ according to Assumption 1. Since $\boldsymbol{R}$ is a diagonal positive-definite matrix, then it is clear that matrix $\boldsymbol{D}$ is a positive-definite diagonal matrix, with eigenvalues of the form

$$\lambda_{Dk} = \frac{1}{2\sum_{k=1}^{n+m} 1/R_k}\left(\frac{1}{R_k} + \frac{\sum_{k=1}^{n+m} V_k/R_k}{\sqrt{\left(\sum_{k=1}^{n+m} V_{ke}/R_k\right)^2 - 4P\sum_{k=1}^{n+m} 1/R_k}}\frac{1}{R_k}\right),$$
$$\forall k = 1, \dots, n+m.$$

3 Nonlinear control design and analysis

3.1 Proposed controller

The purpose of the designed controller is to achieve accurate distribution of the load power and tight load voltage regulation close to the rated value, ensuring that the current of each converter does not violate certain bounds. The proposed concept is based on the idea of partially decoupling the inductor current dynamics, introducing a constant virtual resistance with a bounded controllable voltage for both the bidirectional three-phase AC/DC and the DC/DC boost converters. In both cases, the dynamics of the controllable virtual voltage will guarantee the desired upper bound for the converters' currents regardless of the direction of the power flow.

3.1.1 Three-phase rectifier: Although a current-limiting controller was recently proposed in [39], it only allows unidirectional power flow, which is a significant limitation when storage units are introduced or the AC/DC converter represents an interface between a DC and an AC micro-grid. To overcome this problem, here the control inputs m_{di} and m_{qi}, with $i \in \{1, 2, \dots, n\}$ are proposed to take the following form

$$m_{di} = \frac{2}{V_i}(U_{di} - E_{di} - \omega_i L_{si} I_{qi} + r_{vi} I_{di}) \tag{12}$$

$$m_{qi} = \frac{2}{V_i}(\omega_i L_{si} I_{di} + r_{vi} I_{qi}) \tag{13}$$

where $r_{vi} > 0$ is a constant virtual resistance and E_{di} a virtual voltage that change according to the following nonlinear dynamics:

$$\dot{E}_{di} = c_{di}\left(V^* - V_L - d_i\left(\frac{3}{2}\frac{U_{di}E_{di}}{r_{vi}} - P_{\mathrm{set}i}\right)\right)E_{dqi}^2 \tag{14}$$

$$\begin{aligned}\dot{E}_{dqi} = &-c_{di}\left(V^* - V_L - d_i\left(\frac{3}{2}\frac{U_{di}E_{di}}{r_{vi}} - P_{\mathrm{set}i}\right)\right)\frac{E_{di}E_{dqi}}{E_{\max i}^2} \\ &-k_i c_{di}\left(\frac{E_{di}^2}{E_{\max i}^2} + E_{dqi}^2 - 1\right)E_{dqi}\end{aligned} \tag{15}$$

with E_{dqi} representing an additional control state, V^* the load voltage reference, $P_{\mathrm{set}i}$ the set output power, d_i the droop

This is an open access article published by the IET under the Creative Commons Attribution License (http://creativecommons.org/licenses/by/3.0/)

$$\boldsymbol{Y}=\frac{\partial i_k}{\partial V_k}=\begin{bmatrix}\frac{1}{R_1}\left(1-\frac{\partial V_L}{\partial V_1}\right) & -\frac{1}{R_1}\frac{\partial V_L}{\partial V_2} & \cdots & -\frac{1}{R_1}\frac{\partial V_L}{\partial V_{n+m}}\\ -\frac{1}{R_2}\frac{\partial V_L}{\partial V_1} & \frac{1}{R_2}\left(1-\frac{\partial V_L}{\partial V_2}\right) & \cdots & -\frac{1}{R_2}\frac{\partial V_L}{\partial V_{n+m}}\\ \vdots & \vdots & \ddots & \vdots\\ -\frac{1}{R_{n+m}}\frac{\partial V_L}{\partial V_1} & -\frac{1}{R_{n+m}}\frac{\partial V_L}{\partial V_2} & \cdots & \frac{1}{R_{n+m}}\left(1-\frac{\partial V_L}{\partial V_{n+m}}\right)\end{bmatrix}$$
$$=\begin{bmatrix}\frac{1}{R_1} & 0 & \cdots & 0\\ 0 & \frac{1}{R_2} & \cdots & 0\\ \vdots & \vdots & \ddots & \vdots\\ 0 & 0 & \cdots & \frac{1}{R_{n+m}}\end{bmatrix}\left(I_{n+m}-1_{(n+m)\times(n+m)}\begin{bmatrix}\frac{\partial V_L}{\partial V_1} & 0 & \cdots & 0\\ 0 & \frac{\partial V_L}{\partial V_2} & \cdots & 0\\ \vdots & \vdots & \ddots & \vdots\\ 0 & 0 & \cdots & \frac{\partial V_L}{\partial V_{n+m}}\end{bmatrix}\right) \tag{10}$$
$$=R^{-1}\left(I_{n+m}-1_{(n+m)\times(n+m)}\boldsymbol{D}\right)$$

$$\boldsymbol{D}=\begin{bmatrix}\frac{\partial V_L}{\partial V_1} & \cdots & 0\\ \vdots & \ddots & \vdots\\ 0 & \cdots & \frac{\partial V_L}{\partial V_{n+m}}\end{bmatrix}=\frac{1}{2\sum_{k=1}^{n+m}1/R_k}\left(R^{-1}+\frac{\sum_{k=1}^{n+m}V_k/R_k}{\sqrt{\left(\sum_{k=1}^{n+m}V_k/R_k\right)^2-4P\sum_{k=1}^{n+m}1/R_k}}\begin{bmatrix}\frac{1}{R_1} & \cdots & 0\\ \vdots & \ddots & \vdots\\ 0 & \cdots & \frac{1}{R_{n+m}}\end{bmatrix}\right) \tag{11}$$
$$=\frac{1}{2\sum_{k=1}^{n+m}1/R_k}\left(R^{-1}+\frac{\sum_{k=1}^{n+m}V_k/R_k}{\sqrt{\left(\sum_{k=1}^{n+m}V_k/R_k\right)^2-4P\sum_{k=1}^{n+m}1/R_k}}R^{-1}\right)$$

coefficient, and c_{di}, $E_{\max i}$, k_i being positive constants. The proposed controller introduces the desired droop expression via the input m_{di}, while it forces the current I_{qi} to zero through m_{qi} in order to guarantee unity power factor operation, since $Q_i=(3/2)U_{di}I_{qi}$.

3.1.2 Bidirectional DC/DC boost converter: Following a similar control framework with the AC/DC converter, for the DC/DC boost converter the control input u_j, with $j\in\{n+1,\ldots,n+m\}$, becomes

$$u_j=1-\frac{r_{vj}i_{Lj}+U_j-E_j}{V_j} \tag{16}$$

where $r_{vbj}>0$ represents a constant virtual resistance and E_j a virtual controllable voltage

$$\dot{E}_j=c_j\left(V^*-V_L-d_j\left(\frac{U_jE_j}{r_{vbj}}-P_{\text{set}j}\right)\right)E_{bqj}^2 \tag{17}$$

$$\dot{E}_{bqj}=-c_j\left(V^*-V_L-d_j\left(\frac{U_jE_j}{r_{vbj}}-P_{\text{set}j}\right)\right)\frac{E_jE_{bqj}}{E_{\max j}^2}-k_jc_j\left(\frac{E_j^2}{E_{\max j}^2}+E_{bqj}^2-1\right)E_{bqj} \tag{18}$$

where E_{bqj} being an additional control state, $P_{\text{set}j}$ the set output power, d_j the droop coefficient, and c_j, k_j, $E_{\max j}$ positive constants. Compared to the robust droop controller [11], the proposed strategy does not require the measurement of the output current i_i, i_j of each converter, thus leading to a simpler implementation. It is highlighted that a second controller state E_{dq}, E_{bq} is based on the bounded integral controller concept [43]. For more details on the bounded dynamics of the control states the reader is referred to [43] where it is shown that the control states are guaranteed to stay within their imposed bounds $E_{di}\in[-E_{\max i},E_{\max i}]$, $E_j\in\left[-E_{\max j},E_{\max j}\right]$ and $E_{dqi},E_{bqj}\in[0,1]$ for all $t\geq 0$, given typical initial conditions $E_{di}=E_j=0$ and $E_{dqi}=E_{bqj}=1$. The block diagram depicting the controller implementation, measurement and actuation parts is presented in Fig. 3. Having introduced the proposed control schemes, consider the additional assumptions for the system:

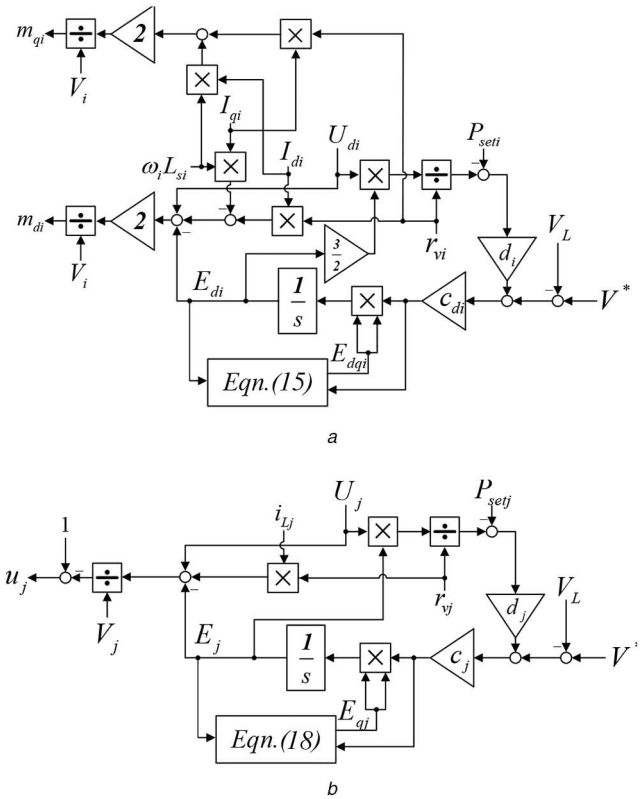

Fig. 3 *Block diagram with the control implementation of the proposed controllers*
(a) 3-phase bidirectional rectifier controller, ***(b)*** DC/DC bidirectional boost converter controller

This is an open access article published by the IET under the Creative Commons Attribution License (http://creativecommons.org/licenses/by/3.0/)

Assumption 3: For every constant $E_{die} \in (-E_{\max i}, E_{\max i})$ and $E_{je} \in (-E_{\max j}, E_{\max j})$, satisfying

$$\begin{aligned} & d_{d1}\frac{3}{2}\left(\frac{U_{d1}E_{d1e}}{r_{vd1}} - P_{set1}\right) = \ldots = d_{dn}\frac{3}{2}\left(\frac{U_{dn}E_{dne}}{r_{vdn}} - P_{setn}\right) \\ & = d_{n+1}\left(\frac{U_{n+1}E_{(n+1)e}}{r_{v(n+1)}} - P_{set(n+1)}\right) = \ldots \\ & = d_{n+m}\left(\frac{U_{n+m}E_{(n+m)e}}{r_{v(n+m)}} - P_{set(n+m)}\right) \end{aligned} \tag{19}$$

there exists a unique steady-state equilibrium point $(I_{die}, I_{qie}, i_{Lje}, V_{ie}, V_{je}, E_{die}, E_{dqie}, E_{je}, E_{bqje})$ corresponding to a load voltage regulation, V_{Le}, where $E_{dqie}, E_{bqje} \in (0, 1], \forall k = 1, \ldots, n+m$.

Assumption 4: For $\forall k = 1 \ldots n+m$ it holds that $(U_k d_k)/(\alpha_k R_k) > 0$, with $\alpha_k = 3$ when $k = 1 \ldots n$ and $\alpha_k = 1$ when $k = n+1 \ldots n+m$.

For the selection of $E_{\max i}$ and $E_{\max j}$ the following condition should hold

$$|E_{\max k}| < U_k, \quad \forall k = 1 \ldots n+m\,.$$

The desired current-limiting property for each converter can be now investigated in the next subsection.

3.2 Current limitation

3.2.1 Three-phase rectifier: For system (1)–(2), consider the following continuously differentiable function:

$$V_i = \frac{1}{2}L_{si}I_{di}^2 + \frac{1}{2}L_{si}I_{qi}^2\,. \tag{20}$$

Substituting m_d, m_q from (12) and (13) into (1) and (2), and taking into account that $E_{di} \in [-E_{\max i}, E_{\max i}]$ and $E_{dqi} \in [0, 1]$, the time derivative of V_i becomes

$$\begin{aligned} & \dot{V}_i = L_{si}I_{di}\dot{I}_{di} + L_{si}I_{qi}\dot{I}_{qi} = -r_{vi}I_{di}^2 + E_{di}I_{di} - r_{vi}I_{qi}^2 \\ & \leq -r_{vi}\left(I_{di}^2 + I_{qi}^2\right) + |E_{di}||I_{di}| \\ & \leq -r_{vi}\| I \|_2^2 + |E_{di}|\| I \|_2 \end{aligned}$$

where $I = \left[I_{di}\ I_{qi}\right]^{\mathrm{T}}$. Consider now that $r_{vi} = \bar{r}_{vi} + \varepsilon_i > 0$ for an arbitrarily small ε_i. Then

$$\dot{V}_i \leq -\varepsilon_i\| I \|_2^2, \| I \|_2 \geq \frac{|E_{di}|}{\bar{r}_{vi}} \tag{21}$$

which means that system (1)–(2) is ISS [44] with respect to the virtual voltage E_{di}. Since E_{di} is bounded below the chosen maximum virtual voltage value $E_{\max i}$, then both the d and q currents, I_d and I_q will remain bounded at all times.

Since $I = \left[I_d\ I_q\right]^{\mathrm{T}}$ then taking into account the dq transformation, it results in

$$\| I \|_2 = \sqrt{I_{di}^2 + I_{qi}^2} = \sqrt{\left(\sqrt{2}I_{\mathrm{rms}}\right)^2} = \sqrt{2}I_{\mathrm{rms}}\,. \tag{22}$$

For

$$I_{\mathrm{rms}}^{\max} = \frac{E_{\max i}}{\bar{r}_{vi}} \tag{23}$$

it is proven from the ISS property (21) that if initially the RMS AC/DC converter current is below the maximum allowed value $I_{\mathrm{rms}}^{\max}$, i.e. $I_{\mathrm{rms}}(0) < I_{\mathrm{rms}}^{\max}$, then

$$I_{\mathrm{rms}}(t) \leq \frac{E_{\max i}}{\bar{r}_{vi}} = I_{\mathrm{rms}}^{\max}, \quad \forall t \geq 0.$$

Hence, the input current of each rectifier separately is always limited below $I_{\mathrm{rms}}^{\max}$ with the appropriate choice of $E_{\max i}$ and r_{vi} given in (23), ensuring protection at all times. It is shown that the current-limiting property of each converter is guaranteed independently from the power sharing expression $V^* - V_L - d_i((3/2)(U_{di}E_{di}/r_{vi}) - P_{seti})$ that has to be regulated to zero. This means that each converter has as first priority to protect itself from high currents that can damage the device. When the current is below the maximum value, the converter contributes to the desired power sharing within the DC micro-grid.

3.2.2 Bidirectional boost converter: By applying the proposed controller expression (16) into the bidirectional converters dynamics (4), the closed-loop system equation for the inductor current i_L takes the following form

$$L\dot{i}_L = -r_{vb}i_L + E_b, \tag{24}$$

where $r_{vb} = \mathrm{diag}\{r_{vbj}\}$ and $E_b = [E_{n+1} \ldots E_{n+m}]^{\mathrm{T}}$. One can clearly see that r_{vb} represents a constant virtual resistance in series with the converter inductor L.

To investigate how the selection of the virtual resistance and the bounded controller dynamics of E are related to the desired overcurrent protection, let the following continuously differentiable function:

$$V_j = \frac{1}{2}L_j i_{Lj}^2$$

for closed-loop current dynamics (24). The time derivative of V_j yields

$$\begin{aligned} & \dot{V}_j = L_j i_{Lj}\dot{i}_{Lj} = -r_{vbj}i_{Lj}^2 + E_j i_{Lj} \\ & \leq -r_{vbj}i_{Lj}^2 + |E_j||i_{Lj}|\,. \end{aligned}$$

Considering $r_{vbj} = \bar{r}_{vbj} + \varepsilon_j > 0$ for arbitrarily small ε_j, then

$$\dot{V}_j \leq -\varepsilon_j i_L^2, \quad \forall |i_L| \geq \frac{|E_j|}{\bar{r}_{vbj}}, \tag{25}$$

which means that system (24) is ISS with respect to the bounded virtual voltage, E_j. Similar to the rectifier case, since $|E_j| \in \left[-E_{\max j}, E_{\max j}\right]$ then

$$i_L \leq \frac{E_{\max j}}{\bar{r}_{vbj}}, \quad \forall t > 0, \tag{26}$$

holds true if initially the inductor current is below the same value, i.e. $i_L(0) < E_{\max j}/\bar{r}_{vbj}$.

Hence one can clearly select the parameters $E_{\max j}$ and $\bar{r}_{vbj}$ in the proposed controller in order to satisfy

$$E_{\max j} = \bar{r}_{vbj}i_L^{\max}, \tag{27}$$

and guarantee that

$$|i_L(t)| \leq i_L^{\max}, \quad \forall t > 0. \tag{28}$$

Any selection of the constant and positive parameters $E_{\max j}$ and $\bar{r}_{vbj}$ that satisfy (27) results in the desired overcurrent protection (28) of the converter's inductor current regardless the load magnitude or system parameters.

It is underlined that compared to existing conventional overcurrent protection control strategies, here it has been mathematically proven according to the nonlinear ISS theory that

This is an open access article published by the IET under the Creative Commons Attribution License (http://creativecommons.org/licenses/by/3.0/)

the proposed controller maintains the current limited during transients and does not require limiters or saturation units which are prone to yield instability in the system. At the same time, it maintains the continuous time structure of the closed-loop system that facilitates the stability analysis that follows.

4 Stability analysis

By applying the proposed controller (12)–(15), (16)–(18) into the DC micro-grid dynamics (1)–(3), (4)–(5) the closed-loop system can be written in the following matrix form:

$$\begin{bmatrix}\dot{I}_d\\ \dot{I}_q\\ \dot{i}_L\\ \dot{V}_r\\ \dot{V}_b\end{bmatrix}=\begin{bmatrix}L_s^{-1}(-r_{vd}I_d+E_d)\\ -L_s^{-1}r_{vd}I_q\\ L_b^{-1}(-r_{vb}i_L+E_b)\\ \frac{3}{2}C_r^{-1}[V_r]^{-1}(([U_d]-[E_d]+r_{vd}[I_d])I_d-r_{vd}I_q^2)-C_r^{-1}i_r\\ C_b^{-1}[V_b]^{-1}(r_{vb}[i_L]+[U_b]-[E_b])i_L-C_b^{-1}i_b\end{bmatrix} \tag{29}$$

(see (30))

where $d_d=\mathrm{diag}\{d_i\}$, $d_b=\mathrm{diag}\{d_j\}$, $k_d=\mathrm{diag}\{k_i\}$, $k_b=\mathrm{diag}\{k_j\}$, $E_d=[E_{d1}\ldots E_{dn}]^{\mathrm{T}}$, $E_{dq}=[E_{dq1}\ldots E_{dqn}]^{\mathrm{T}}$, $E_{bq}=[E_{bq(n+1)}\ldots E_{bq(n+m)}]^{\mathrm{T}}$, $r_{vd}=\mathrm{diag}\{r_{vi}\}$, $c_d=\mathrm{diag}\{c_{di}\}$, $c_b=\mathrm{diag}\{c_j\}$, $E_{\max d}=\mathrm{diag}\{E_{\max i}\}$, $E_{\max b}=\mathrm{diag}\{E_{\max j}\}$, $P_{\mathrm{set}d}=[P_{\mathrm{set}1}\ldots P_{\mathrm{set}n}]^{\mathrm{T}}$, $P_{\mathrm{set}b}=[P_{\mathrm{set}(n+1)}\ldots P_{\mathrm{set}(n+m)}]^{\mathrm{T}}$.

Consider an equilibrium point $\left[I_{de}^{\mathrm{T}}\ I_{qe}^{\mathrm{T}}\ i_{Le}^{\mathrm{T}}\ V_{re}^{\mathrm{T}}\ V_{be}^{\mathrm{T}}\ E_{de}^{\mathrm{T}}\ E_{dqe}^{\mathrm{T}}\ E_{be}^{\mathrm{T}}\ E_{bqe}^{\mathrm{T}}\right]$ calculated from (29)–(30) at the steady-state, satisfying Assumption 3. By setting $\varepsilon=1/\min\{c_k\}$, there exists $\delta_d=\mathrm{diag}\{\delta_i\}\geq 0$ and $\delta=\mathrm{diag}\{\delta_j\}\geq 0$ such that $c_d=(1/\varepsilon)I_n+\delta_d$ and $c_b=(1/\varepsilon)I_m+\delta$. Thus (30) becomes (see (31)) , where $\bar{\delta}=\mathrm{diag}\{\delta_d,\delta\}$, $d=\mathrm{diag}\{d_k\}$, $k=\mathrm{diag}\{k_k\}$, $E=[E_d^{\mathrm{T}}E_b^{\mathrm{T}}]^{\mathrm{T}}$, $E_q=[E_{dq}^{\mathrm{T}}E_{bq}^{\mathrm{T}}]^{\mathrm{T}}$, $r_v=\mathrm{diag}\{r_{vk}\}$, $U=[U_d^{\mathrm{T}}U_b^{\mathrm{T}}]^{\mathrm{T}}$, $E_{\max}=\mathrm{diag}\{E_{\max k}\}$, $P_{\mathrm{set}}=[P_{\mathrm{set}d}^{\mathrm{T}}P_{\mathrm{set}b}^{\mathrm{T}}]^{\mathrm{T}}$.

Hence, the closed-loop system equations and can be written as

$$\dot{x}=f(x,z) \tag{32}$$

$$\varepsilon\,\dot{z}=g(x,z,\varepsilon) \tag{33}$$

where

$$x=\begin{bmatrix}I_d-I_{de}\\ I_q\\ i_L-i_{Le}\\ V_r-V_{re}\\ V_b-V_{be}\end{bmatrix}\ \text{and}\ z=\begin{bmatrix}E_d-E_{de}\\ E_{dq}-E_{dqe}\\ E-E_e\\ E_{bq}-E_{bqe}\end{bmatrix}.$$

For arbitrarily large values of the controller gains c_d, c_b the value of ε is small and therefore (32)–(33) can be investigated as a singularly perturbed system using two-time-scale analysis [44]. The controller's system (31) is also referred to as the boundary layer since it represents the immediate vicinity of a bounding surface where the effects of stability are significant.

Considering f, g being continuously differentiable in the domain $(x,z,\varepsilon)\in D_x\times D_z\times[0,\varepsilon_0]$, when the controller gains c_d, c_b are selected sufficiently large, then $\varepsilon\to 0$ and, based on singular perturbation theory, g will have an algebraic form of $0=g(x,z)$ (see (34)) . The roots of the above system can be computed as shown below

$$\begin{bmatrix}\overline{E}\\ \overline{E}_q\end{bmatrix}=\begin{bmatrix}\begin{bmatrix}\frac{2}{3}I_n & \mathbb{O}_{n\times m}\\ \mathbb{O}_{m\times n} & I_m\end{bmatrix}r_v[U]^{-1}\left(d^{-1}(V^*-V_L)1_{n+m}+P_{\mathrm{set}}\right)\\ \left(I_{n+m}-E_{\max}^{-2}\left[\overline{E}\right]^2\right)^{-1/2}1_{n+m}\end{bmatrix} \tag{35}$$

These roots can also be written as $z=h(x)$ with $\overline{E}_{di}\in(-E_{\max i},E_{\max i})$, $\overline{E}_{je}\in(-E_{\max j},E_{\max j})$, and $\overline{E}_{dqie},\overline{E}_{bqje}\in[0,1]$, such that $h(0)=0$. Thus, the roots also represent the equilibrium points of the nonlinear system. Exponential stability at the origin can be investigated via system's (33) corresponding Jacobian matrix (see (36)) , where it is obvious that J_1 has negative eigenvalues since it is lower triangular and the diagonal elements

$$-\begin{bmatrix}\frac{3}{2}I_n & \mathbb{O}_{n\times m}\\ \mathbb{O}_{m\times n} & I_m\end{bmatrix}d\left[E_{qe}\right]^2[U]r_v^{-1}\ \text{and}\ -2k\left[E_{qe}\right]^2$$

are diagonal and negative definite matrices.

Therefore matrix $\boldsymbol{J}_1$ is Hurwitz. Hence, there exist $\rho_1>0$ and a domain $\tilde{D}_z=\{z\epsilon R^{2n},\|\ z\ \|_2<\rho_1\}$ where $\tilde{D}_z\subseteq D_z$ such that (33) is exponentially stable at the origin uniformly in x.

To obtain the reduced model, the roots $\overline{E}$ and $\overline{E}_q$ are substituted from (35) into (29), yielding (see (37)) , with $i_{in}=\left[I_d^{\mathrm{T}}i_L^{\mathrm{T}}\right]^{\mathrm{T}}$, $V=\left[V_r^{\mathrm{T}}V_b^{\mathrm{T}}\right]^{\mathrm{T}}$, $i=\left[i_r^{\mathrm{T}}i_b^{\mathrm{T}}\right]^{\mathrm{T}}$, $C=\mathrm{diag}\{C_k\}$, $L=\mathrm{diag}\{L_k\}$.

In the literature, the above model is referred to as quasi-steady-state model, since $\overline{E}$ and $\overline{E_q}$ introduce a velocity $\left[\dot{\overline{E}}\ \ \dot{\overline{E}}_q\right]=\varepsilon^{-1}g$ that

$$\begin{bmatrix}\dot{E}_d\\ \dot{E}_{dq}\\ \dot{E}_b\\ \dot{E}_{bq}\end{bmatrix}=\begin{bmatrix}c_d\left[E_{dq}\right]^2\left(V^*1_n-V_L1_n-d_d\left(\frac{3}{2}r_{vd}^{-1}[U_d]E_d-P_{\mathrm{set}d}\right)\right)\\ -c_dE_{\max d}^{-2}[E_d]\left[E_{dq}\right]\left(V^*1_n-V_L1_n-d_d\left(\frac{3}{2}r_{vd}^{-1}[U_d]E_d-P_{\mathrm{set}d}\right)\right)-k_dc_d\left(E_{\max d}^{-2}[E_d]^2+\left[E_{dq}\right]^2-I_n\right)E_{dq}\\ c_b\left[E_{bq}\right]^2\left(V^*1_m-V_L1_m-d_b\left(r_{vb}^{-1}[U_b]E_b-P_{\mathrm{set}b}\right)\right)\\ -c_bE_{\max b}^{-2}[E_b]\left[E_{bq}\right]\left(V^*1_m-V_L1_m-d_b\left(r_{vb}^{-1}[U_b]E_b-P_{\mathrm{set}b}\right)\right)-k_bc_b\left(E_{\max b}^{-2}[E_b]^2+\left[E_{bq}\right]^2-I_m\right)E_{bq}\end{bmatrix} \tag{30}$$

$$\begin{bmatrix}\varepsilon\dot{E}\\ \varepsilon\dot{E}_q\end{bmatrix}=\begin{bmatrix}I_{n+m}+\bar{\delta} & \mathbb{O}_{(n+m)\times(n+m)}\\ \mathbb{O}_{(n+m)\times(n+m)} & I_{n+m}+\bar{\delta}\end{bmatrix}\times\begin{bmatrix}\left[E_q\right]^2\left((V^*-V_L)1_{n+m}-d\left(\begin{bmatrix}\frac{3}{2}I_n & \mathbb{O}_{n\times m}\\ \mathbb{O}_{m\times n} & I_m\end{bmatrix}r_v^{-1}[U]E-P_{\mathrm{set}}\right)\right)\\ -E_{\max}^{-2}[E]\left[E_q\right]\left((V^*-V_L)1_{n+m}-d\left(\begin{bmatrix}\frac{3}{2}I_n & \mathbb{O}_{n\times m}\\ \mathbb{O}_{m\times n} & I_m\end{bmatrix}r_v^{-1}[U]E-P_{\mathrm{set}}\right)\right)\\ -k\left(E_{\max}^{-2}[E]^2+\left[E_q\right]^2-I_{n+m}\right)E_q\end{bmatrix} \tag{31}$$

This is an open access article published by the IET under the Creative Commons Attribution License (http://creativecommons.org/licenses/by/3.0/)

is very large when ε is small and $g \neq 0$, leading to fast convergence to a root $h(I_d, I_q, i_L, V_r, V_b)$, which also represents the equilibrium of the boundary-layer.

The second equation of (29) is independent, thus there are n eigenvalues where $\lambda_i = -r_{vi}/L_{si} < 0$. The corresponding Jacobian matrix of the reduced system (37) that remains to be investigated will have the form of J_2 (see equation below), with $\boldsymbol{A}$ and $\boldsymbol{B}$ being

$$\boldsymbol{A} = \begin{bmatrix} \frac{2}{3}I_n & \mathbb{O}_{n\times m} \\ \mathbb{O}_{m\times n} & I_m \end{bmatrix} r_v[U]^{-1}d^{-1}1_{(n+m)\times(n+m)}$$

$$\boldsymbol{B} = \begin{bmatrix} 3I_n & \mathbb{O}_{n\times m} \\ \mathbb{O}_{m\times n} & I_m \end{bmatrix} C^{-1}[V_e]^{-1}$$

The characteristic polynomial can be calculated from

$$\left|\lambda I_{2(n+m)} - J_2\right| = \left|\lambda^2 I_{n+m} + \lambda\mathbb{C}\boldsymbol{D} + \mathbb{K}\boldsymbol{D}\right| = 0,$$

with $\mathbb{C}$ and $\mathbb{K}$ expressed (see (38)) . Following factorisation the matrices $\mathbb{C}$ and $\mathbb{K}$ become as presented (see (39)) , with

$$\mathbb{Q}_1 = \boldsymbol{B}\begin{bmatrix} \frac{2}{3}I_n & \mathbb{O}_{n\times m} \\ \mathbb{O}_{m\times n} & I_m \end{bmatrix} r_v[U]^{-1}d^{-1} + C^{-1}R^{-1}$$

$$\mathbb{Q}_2 = C^{-1}R^{-1} - \begin{bmatrix} \frac{2}{3}I_n & \mathbb{O}_{n\times m} \\ \mathbb{O}_{m\times n} & I_m \end{bmatrix}\boldsymbol{B}d^{-1}$$

Let the characteristic polynomial be

$$\left|\lambda^2\boldsymbol{D}^{-1} + \lambda\mathbb{C} + \mathbb{K}\right|\left|\boldsymbol{D}\right| = 0.$$

Considering $\mathbb{G} = L^{-1}r_v\mathbb{Q}_2$, the characteristic polynomial becomes

$$|\mathbb{G}|\left|\lambda^2\mathbb{G}^{-1}\boldsymbol{D}^{-1} + \lambda\tilde{\mathbb{C}} + \tilde{\mathbb{K}}\right|\left|\boldsymbol{D}\right| = 0.$$

with $\tilde{\mathbb{C}} = \mathbb{G}^{-1}\mathbb{C}$ and $\tilde{\mathbb{K}} = \mathbb{G}^{-1}\mathbb{K}$. As the determinants $|\mathbb{G}|$ and $|D|$ are positive, the polynomial reduces to

$$\left|\lambda^2\mathbb{G}^{-1}\boldsymbol{D}^{-1} + \lambda\tilde{\mathbb{C}} + \tilde{\mathbb{K}}\right| = 0,$$

which is a quadratic eigenvalue problem (QEP) with $\tilde{\mathbb{K}}$ symmetrical, and $\tilde{\mathbb{C}}$, according to *Lemma 2* in [20], diagonalisable whose eigenvalues are all real, since it is a product of a positive-definite diagonal and a symmetrical matrix.

The characteristic equation then becomes

$$\begin{bmatrix} \mathbb{O}_{n+m} \\ \mathbb{O}_{n+m} \end{bmatrix} = \begin{bmatrix} [E_q]^2\left((V^* - V_L) - 1_{n+m} - d\left(\begin{bmatrix} \frac{3}{2}I_n & \mathbb{O}_{n\times m} \\ \mathbb{O}_{m\times n} & I_m \end{bmatrix} r_v^{-1}[U]E - P_{\text{set}}\right)\right) \\ -E_{\max}^{-2}[E][E_q]\left((V^* - V_L)1_{-n+m} - d\left(\begin{bmatrix} \frac{3}{2}I_n & \mathbb{O}_{n\times m} \\ \mathbb{O}_{m\times n} & I_m \end{bmatrix} r_v^{-1}[U]E - P_{\text{set}}\right)\right) - k\left(E_{\max}^{-2}[E]^2 + [E_q]^2 - I_m\right)E_q \end{bmatrix} \tag{34}$$

$$\boldsymbol{J}_1 = \begin{bmatrix} -\begin{bmatrix} \frac{3}{2}I_n & \mathbb{O}_{n\times m} \\ \mathbb{O}_{m\times n} & I_m \end{bmatrix} d[E_{qe}]^2[U]r_v^{-1} & \mathbb{O}_{(n+m)\times(n+m)} \\ \left(\left(\begin{bmatrix} \frac{3}{2}I_n & \mathbb{O}_{n\times m} \\ \mathbb{O}_{m\times n} & I_m \end{bmatrix} d[U]r_v^{-1} - 2k\right)[E_e][E_{qe}]E_{\max}^{-2}\right. & \left. -2k[E_{qe}]^2 \right) \end{bmatrix} \tag{36}$$

$$\begin{bmatrix} \dot{i}_{in} \\ \dot{V} \end{bmatrix} = \begin{bmatrix} L^{-1}\left(-r_v i_{in} + \overline{E}\right) \\ \begin{bmatrix} 3I_n & \mathbb{O}_{n\times m} \\ \mathbb{O}_{m\times n} & I_m \end{bmatrix} C^{-1}[V]^{-1}\left(([U] - [\overline{E}] + r_v[i_{in}])i_{in} - \begin{bmatrix} r_v I_q^2 & \mathbb{O}_{n\times m} \\ \mathbb{O}_{m\times n} & \mathbb{O}_{m\times m} \end{bmatrix}\right) - C^{-1}i \end{bmatrix} \tag{37}$$

$$\boldsymbol{J}_2 = \begin{bmatrix} -L^{-1}r_v & -L^{-1}\boldsymbol{A}\boldsymbol{D} \\ \boldsymbol{B}([U] + [\overline{E}]) & -\boldsymbol{B}[i_{ine}]([V_e]^{-1}[U] - \boldsymbol{A}\boldsymbol{D}) - C^{-1}R^{-1}(I_{n+m} - 1_{(n+m)\times(n+m)}\boldsymbol{D}) \end{bmatrix}$$

$$\begin{aligned} \mathbb{C} &= L^{-1}r_v\boldsymbol{D}^{-1} + \boldsymbol{B}[i_{ine}]([V_e]^{-1}[U]\boldsymbol{D}^{-1} - \boldsymbol{A}) + C^{-1}R^{-1}\left(\boldsymbol{D}^{-1} - 1_{(n+m)\times(n+m)}\right) \\ \mathbb{K} &= L^{-1}r_v\left(\boldsymbol{B}[i_{ine}][V_e]^{-1}[U]\boldsymbol{D}^{-1} + C^{-1}R^{-1}\left(\boldsymbol{D}^{-1} - 1_{(n+m)\times(n+m)}\right)\right) \\ &\quad + L^{-1}r_v\begin{bmatrix} \frac{2}{3}I_n & \mathbb{O}_{n\times m} \\ \mathbb{O}_{m\times n} & I_m \end{bmatrix}\boldsymbol{B}d^{-1}1_{(n+m)\times(n+m)} \end{aligned} \tag{38}$$

$$\begin{aligned} \mathbb{C} &= \mathbb{Q}_1\left(\mathbb{Q}_1^{-1}\left(L^{-1}r_v\boldsymbol{D}^{-1} + \boldsymbol{B}[i_{ine}][V_e]^{-1}[U]\boldsymbol{D}^{-1} + C^{-1}R^{-1}\boldsymbol{D}^{-1}\right) - 1_{(n+m)\times(n+m)}\right) \\ \mathbb{K} &= L^{-1}r_v\mathbb{Q}_2\left(\mathbb{Q}_2^{-1}\left(\boldsymbol{B}[i_{ine}][V_e]^{-1}[U]\boldsymbol{D}^{-1} + C^{-1}R^{-1}\boldsymbol{D}^{-1}\right) - 1_{(n+m)\times(n+m)}\right) \end{aligned} \tag{39}$$

This is an open access article published by the IET under the Creative Commons Attribution License (http://creativecommons.org/licenses/by/3.0/)

$$\left|\lambda^2\mathbb{G}^{-1}\boldsymbol{D}^{-1}+\lambda\mathbb{P}\Lambda\mathbb{P}^{-1}+\tilde{\mathbb{K}}\right|=0,$$
$$\left|\lambda^2\mathbb{P}^{-1}\mathbb{G}^{-1}\boldsymbol{D}^{-1}\mathbb{P}+\lambda\Lambda+\mathbb{P}^{-1}\tilde{\mathbb{K}}\mathbb{P}\right|=0.$$

Note that $\boldsymbol{\Lambda}$ is a diagonal matrix with the eigenvalues of $\tilde{\mathbb{C}}$ as main entries and the similarity transformations $\mathbb{P}^{-1}\mathbb{G}^{-1}\boldsymbol{D}^{-1}\mathbb{P}$ and $\mathbb{P}^{-1}\tilde{\mathbb{K}}\mathbb{P}$ are symmetrical, as $\mathbb{P}$ is orthogonal $\left(\mathbb{P}^{-1}=\mathbb{P}^{T}\right)$, and they share the same spectrum as $\mathbb{G}^{-1}\boldsymbol{D}^{-1}$ and $\tilde{\mathbb{K}}$, respectively. If $\mathbb{G}^{-1}\boldsymbol{D}^{-1}$, $\boldsymbol{\Lambda}$ and $\tilde{\mathbb{K}}$ are positive-definite, then $\mathrm{Re}(\lambda)<0$ which means that $\boldsymbol{J}_2$ is Hurwitz. Hence, since $\mathbb{G}^{-1}\boldsymbol{D}^{-1}$ is already positive-definite, it is sufficient to show that $\boldsymbol{\Lambda}>0$, or equivalently that $\tilde{\mathbb{C}}$ has positive eigenvalues, and $\tilde{\mathbb{K}}>0$. Since matrix $\tilde{\mathbb{C}}$ is represented by a multiplication where one term is the diagonal matrix $\mathbb{G}^{-1}\mathbb{Q}_1>0$, according to the same *Lemma 2* in [20], the remaining symmetrical term, denoted $\tilde{\mathbb{C}}^*$, will have the same index of inertia as $\tilde{\mathbb{C}}$. The condition $\tilde{\mathbb{C}}^*>0$ becomes

$$\tilde{\mathbb{C}}^*=\mathbb{Q}_1^{-1}\left(L^{-1}r_v\boldsymbol{D}^{-1}+\boldsymbol{B}[i_{ine}][V_e]^{-1}[U]\boldsymbol{D}^{-1}+C^{-1}R^{-1}\boldsymbol{D}^{-1}\right)-1_{(n+m)\times(n+m)}$$

which represents a sum between a diagonal positive-definite real matrix and the real symmetric matrix $-1_{(n+m)\times(n+m)}$. According to *Lemma 1* in [20], if

$$\left(\frac{r_{vk}C_k}{L_k}+\frac{\alpha_k U_k i_{inke}}{V_{ke}^2}+\frac{1}{R_k}\right)\frac{1}{\lambda_{Dk}}-\left(\frac{\beta_k r_{vk}i_{inke}}{V_{ke}U_k d_k}+\frac{1}{R_k}\right)(n+m)>0, \quad (40)$$

$\forall k=1\ldots n+m$ holds, then $\tilde{\mathbb{C}}^*>0$ is satisfied. When $k=1\ldots n$, then $\alpha_k=3$ and $\beta_k=2$, whereas when $k=n+1\ldots n+m$, then $\alpha_k=\beta_k=1$. Regarding condition $\tilde{\mathbb{K}}>0$, taking into account Assumption 4, and according to the same *Lemma 1* if

$$\left(\frac{\alpha_k U_k i_{inke}}{V_{ke}^2}+\frac{1}{R_k}\right)\frac{1}{\lambda_{Dk}}-\left(\frac{1}{R_k}-\frac{\beta_k}{V_{ke}d_k}\right)(n+m)>0, \quad (41)$$

$\forall k=1\ldots n+m$ holds, then $\tilde{\mathbb{K}}>0$ is satisfied. Hence, if the two conditions (38)–(39) are satisfied for each converter then there exist $\rho_2>0$ and a domain $\tilde{D}_x=\left\{x\epsilon R^{2n},\ \|\ x\ \|_2<\rho_2\right\}$ where $\tilde{D}_x\subseteq D_x$ such that the reduced model is exponentially stable at the origin.

According to *Theorem* 11.4 in [44], there exists $\varepsilon^*>0$ such that for all $\varepsilon<\varepsilon^*$ (or equivalently $c_d>(1/\varepsilon^*)I_n+\delta_d$ and $c_b>(1/\varepsilon^*)I_m+\delta$), the equilibrium point $\left[I_{de}^{\mathrm{T}}\ I_{qe}^{\mathrm{T}}\ i_{Le}^{\mathrm{T}}\ V_{re}^{\mathrm{T}}\ V_{be}^{\mathrm{T}}\ E_{de}^{\mathrm{T}}\ E_{dqe}^{\mathrm{T}}\ E_{be}^{\mathrm{T}}\ E_{bqe}^{\mathrm{T}}\right]$ of (32)–(33) with $E_{die}\in\left(-E_i^{\max},E_i^{\max}\right)$, $E_{je}\in\left(-E_j^{\max},E_j^{\max}\right)$ and $E_{dqie},E_{bqje}\in(0,1)$ is exponentially stable; thus completing the stability analysis of the entire DC micro-grid.

5 Validation of closed-loop system stability

To validate the theoretical stability analysis presented in Section 4 and demonstrate how conditions (38)–(39) can be tested, let us consider the system in Section 6 with parameters given in Table 1. Although (38)–(39) might seem difficult to verify, by taking into account that $E_d\in\left[-E_d^{\max},E_d^{\max}\right]$, $E\in\left[-E^{\max},E^{\max}\right]$ and $E_{dq},E_{bq}\in[0,1]$, which is guaranteed by the proposed control design, the procedure to verify whether the system is stable is the following: One can start by selecting a virtual voltage E_{de}, inside its defined range, for the rectifier. Then the values of the equilibrium points of the inductor current and load voltage are computed. Based on these obtained values, the remaining virtual voltages E_e of the DC/DC converter can be calculated. Thereafter, critical points of the output voltages are calculated, followed by the eigenvalues of matrix $\boldsymbol{D}$. Finally, the two conditions can be tested for each converter.

Table 1 Controller and system parameters

Parameters	Values	Parameters	Values
U_{RMS}	110V	U_{bat}	200V
R_{rec}	0.7Ω	R_{bat}	1.2Ω
L_{phase}	2.2mH	L_{bat}	2.3mH
C_{rec}	1200	C_{bat}	2000
d_{rec}	0.015	d_{bat}	0.030
P	200W	k	1000
c_d	2.1	c_{bat}	180
r_v	7Ω	r_{vb}	5Ω
$E_d^{\max}$	21V	$E_b^{\max}$	5V

Hence, following this procedure for different values of the set power of the battery, P_{setBAT}, corresponding to the battery operation, charging and discharging, respectively, one can observe in Fig. 4 that for any E_d in the bounded range $\left(-E_d^{\max},E_d^{\max}\right)=(-21,21)$, the expressions (38)–(39) for each converter are positive, thus guaranteeing closed-loop stability.

To further validate the stability analysis, in Fig. 5, a graphical interpretation of the stability conditions is provided for the entire range of the set power, P_{setBAT}, to visually confirm that the two stability conditions always take positive values in the entire operating range of the particular DC micro-grid (Fig. 6).

6 Simulation results

To test the proposed controller and compare it to the cascaded *PI* approach, a DC micro-grid consisting of a bidirectional boost converter and a three-phase rectifier feeding a CPL is considered having the parameters specified in Table 1. The aim is to achieve tight voltage regulation around the reference value $V^*=400\,\mathrm{V}$, accurate power sharing in a 2:1 ratio among the paralleled AC/DC and DC/DC converters at the load bus while also assuring protection against overcurrents. But first the conditions for stability must hold.

The model has been implemented in Matlab Simulink and simulated for 45 s considering a full testing scenario.

During the first 5 s, the power requested by the load is 200 W and it can be observed in Fig. 7*b* that the load voltage V_L is kept close to the reference value of 400 V, at ∼398 V in both cases. However, the power sharing is only accurately guaranteed (Fig. 7*c*) in a 2:1 manner with the proposed controller having $i_{\mathrm{BAT}}\simeq0.17\,\mathrm{A}$ and $i_{\mathrm{REC}}\simeq0.34\,\mathrm{A}$, unlike the case with cascaded *PI*s where $i_{\mathrm{BAT}}\simeq0.16\,\mathrm{A}$ and $i_{\mathrm{REC}}\simeq0.35\,\mathrm{A}$. The input currents haven't reached their imposed limits yet as shown in Fig. 7*a*.

For the next 20 s the operation principle of the battery is simulated. The direction of the power flow is reversed to allow the battery to charge and discharge. At $t=5\,\mathrm{s}$ the power set by the battery controller becomes negative $P_{\mathrm{setBAT}}=-150\,\mathrm{W}$, thus leaving the battery to be supplied by the three-phase rectifier. The input current of the battery becomes negative, while the rectifier's input current increases to satisfy the new amount of power requested in the network (Fig. 7*a*). The power sharing ratio between the battery and the rectifier disappears since the current of the battery changes its direction, and becomes negative as shown in Fig. 7*a*. The load voltage remains closely regulated to the desired 400 V value, at around 396.5 V in both cases. After 10 s the set value of the power returns to its initial 0 value, allowing the battery to return to its former discharging state. The power sharing ratio comes back to 2:1 as displayed in Fig. 7*c*.

At $t=25\,\mathrm{s}$ the power requested by the load increases $P=400\,\mathrm{W}$ and, thus, more power is needed from the battery and the three-phase rectifier to be injected in the micro-grid. The load voltage drops down to 396 V according to Fig. 7*b* when using the proposed controller and $V_{\mathrm{bat}}=395.5\,\mathrm{V}$ when having cascaded *PI*s. At the same time, the input currents increase and, therefore, the power injected increases at the common bus (Fig. 7*a*). One can see that the sharing is kept between the two sources, the battery and

This is an open access article published by the IET under the Creative Commons Attribution License (http://creativecommons.org/licenses/by/3.0/)

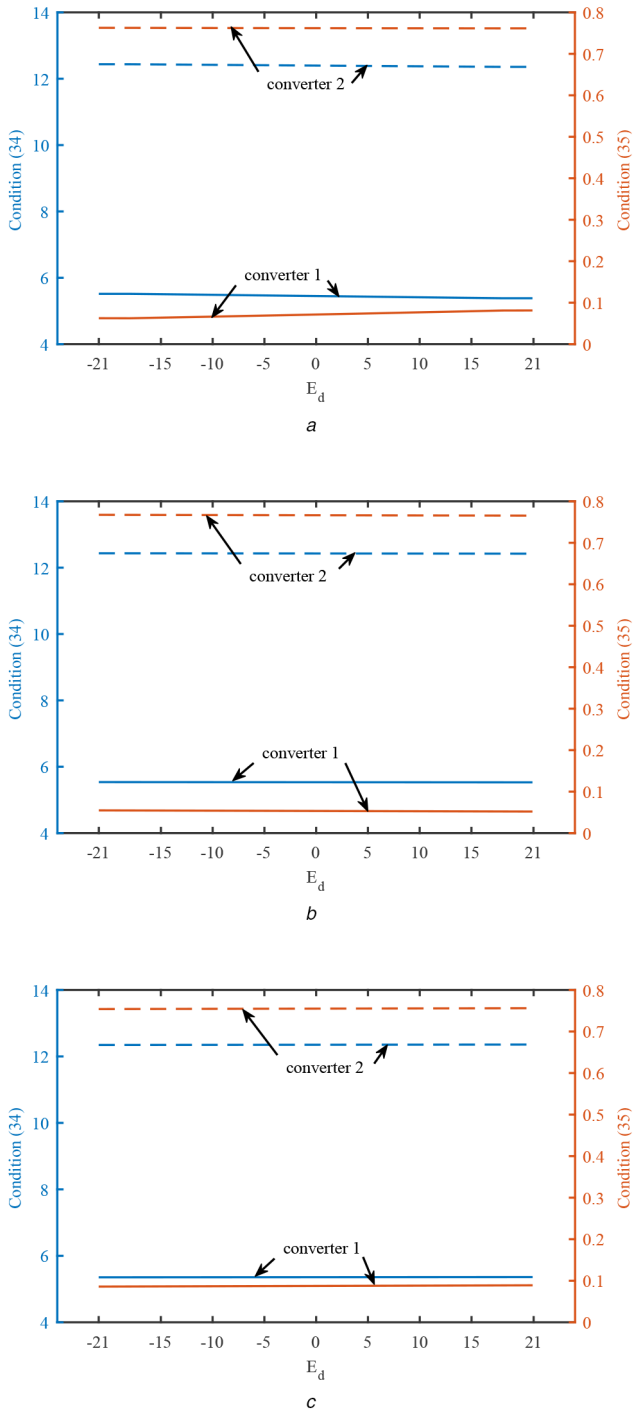

Fig. 4 *Checking stability conditions (38)–(39)*
(a) $P_{\text{setBAT}} = 0\text{W}$, ***(b)*** $P_{\text{setBAT}} = 500\text{W}$, ***(c)*** $P_{\text{setBAT}} = -500\,\text{W}$

rectifier, to the desired proportion of 2:1 having $i_{\text{BAT}} \simeq 0.34\,\text{A}$ and $i_{\text{REC}} \simeq 0.68\,\text{A}$ with the proposed controller, and $i_{\text{BAT}} \simeq 0.32\,\text{A}$ and $i_{\text{REC}} \simeq 0.7\,\text{A}$ with the cascaded *PI* technique, as presented in Fig. 7*c*, given the fact that none of the inductor currents have reached their maximum allowed current. To test the input current protection capability, the power demanded by the load is further increased. Thus, at $t = 35\,\text{s}$ the power requested by the load reaches a higher value than before, $P = 640\,\text{W}$, forcing the battery and the three-phase rectifier to increase their power injection at the load bus. As noticed in Fig. 7*a*, the input current of the battery reaches its limit $i_{\text{LBAT}} = i_{\text{LBAT}}^{\max} = 1\,\text{A}$ without violating it when using the proposed controller, but in the case of the cascaded PIs the transient current exceeds the upper limit prior reaching to steady-state. The power sharing is sacrificed (Fig. 7*c*) to ensure uninterruptible power supply to the load. The load voltage remains within the desired range, $V_L = 393.5\,\text{V}$ with a voltage drop of 6.5

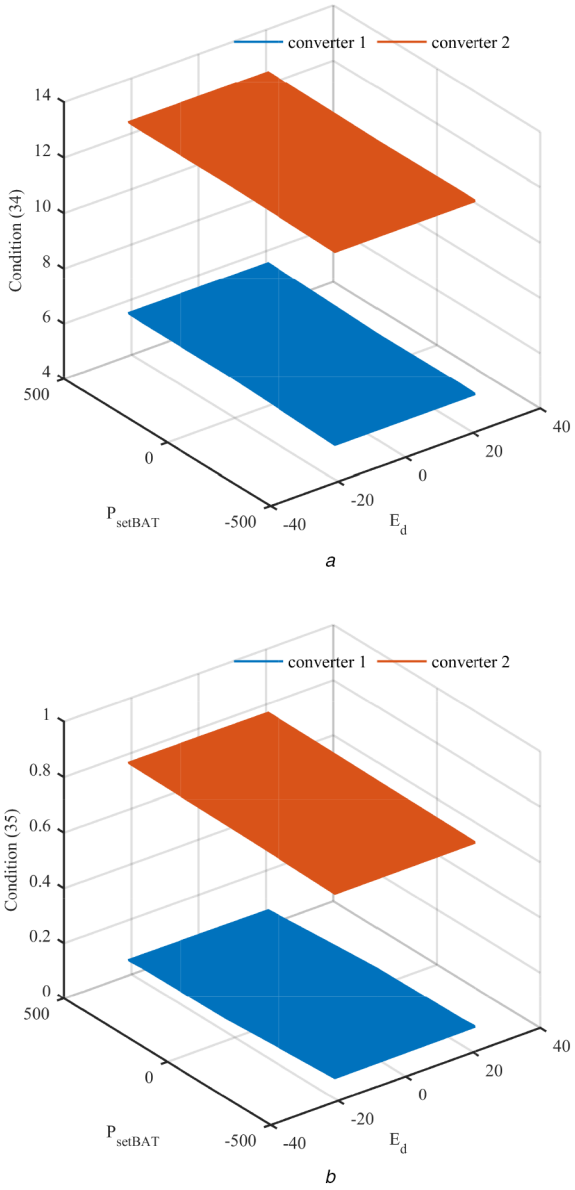

Fig. 5 *Graphical representation of the stability conditions (38)–(39)*
(a) 3D visualisation of condition (38), ***(b)*** 3D visualisation of condition (39)

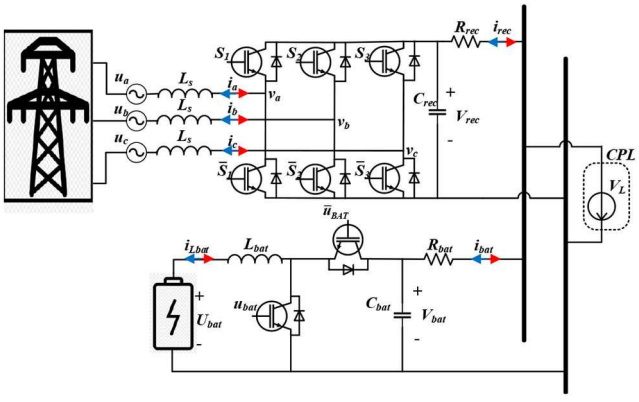

Fig. 6 *DC micro-grid considered for testing, containing a three-phase AC/DC converter connected to the grid, a bidirectional DC/DC boost converter interfacing a battery, and a CPL connected to the main bus and fed by the two converters*

V, which is about 1.5% when having the proposed controller and about $V_L = 392.5\,\text{V}$ with the cascaded *PI* approach.

Consequently, to further verify the theory presented, the controller states E, E_d and E_{dq}, E_{bq} are presented in Figs. 8*a* and *b*. When the input current of the battery reaches its maximum, the

This is an open access article published by the IET under the Creative Commons Attribution License
(http://creativecommons.org/licenses/by/3.0/)

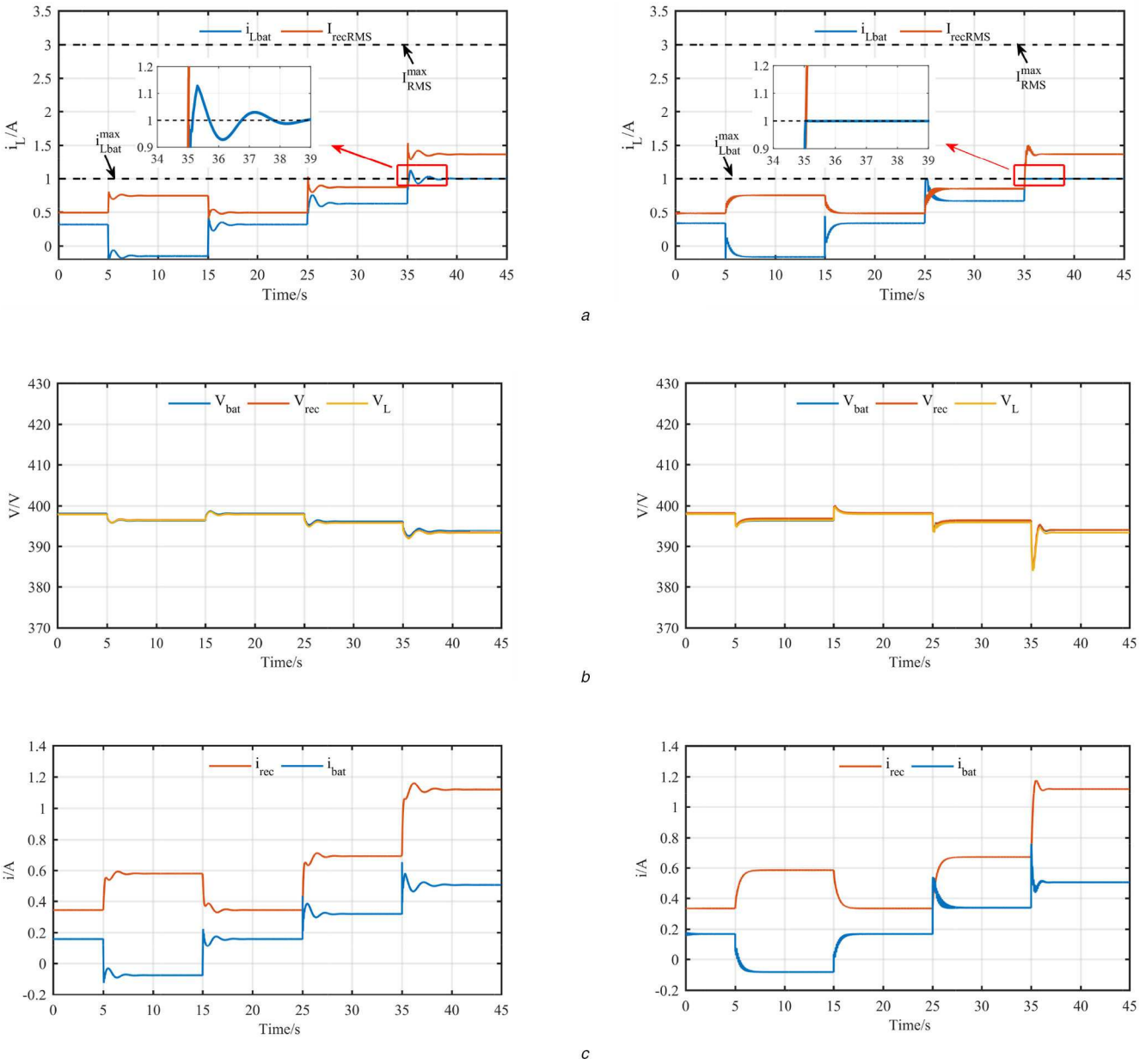

Fig. 7 *Simulation results of the DC micro-grid system with PI cascaded control (left) and the proposed controller (right)*
(a) Inductor currents, ***(b)*** Output voltages, ***(c)*** Output currents

virtual voltage of battery also arrives at its imposed limit $E_b = E_{\max b} = i_L^{\max} r_{vb} = 5\,\text{V}$. One can notice in Fig. 8*b* that the corresponding control state E_{bq} goes to zero when E_b reaches maximum.

It is noted that for the particular DC micro-grid scenario and the parameters used, the closed-loop performance with the cascaded *PI* control remains stable. However, this might not be true for a different system since there is no rigorous proof of stability. On the other hand, the proposed control approach provides a strong theoretic framework, as proven in Section 4, that can be easily tested for different systems as well.

7 Experimental results

A DC micro-grid, with the parameters given in Table 2, consisting of two parallel Texas Instruments DC/DC boost converters connected to a common DC bus and feeding an ETPS ELP-3362F electronic load, operated in CPL mode, is experimentally tested. A switching frequency of 60 kHz was used for the pulse-width-modulation of both converters. The aim is to experimentally validate the proposed nonlinear current-limiting control scheme. The main tasks are to regulate the output voltage to $V^* = 48\,\text{V}$ and regulate the power in a 2:1 ratio, whilst ensuring overcurrent protection.

As one can see in Fig. 9*a*, when the power changes from 40 to 60 W, the voltage is kept close to the reference value of 48 V, while the output currents are accurately shared proportionally to the sources rating, in a 2:1 manner, having $i_2 \simeq 0.45\,\text{A}$ and $i_1 \simeq 0.9\,\text{A}$, provided the input currents, i_{L1} and i_{L2}, have not reached their upper limit.

In Fig. 9*b*, the load power demand decreases from 60 to 40 W. The output currents are accurately shared, having $i_1 \simeq 0.6\,\text{A}$ and $i_2 \simeq 0.3\,\text{A}$, and the load voltage is kept fixed at 48 V.

To test the current-limiting capability, the power increases from 40 to 80 W, as displayed in Fig. 9*c*. One converter reaches to its imposed limit ($i_{L1} \simeq 1.5\,\text{A}$), the power sharing is sacrificed to ensure the uninterrupted power supply of the load. The load voltage is still fairly close to the rated value of 48 V. As it can be seen, the current limitation is not exactly at the 1.5 A limit. This is due to the fact that the parasitic resistance, r_{in}, of the converter's inductance is ignored, in the experiment and the analysis, which in turn causes a slightly lower bound of the input current. If the parasitic resistance is considered, then based on the ISS analysis in Section 3, one can easily obtain that the controller parameters $E^{\max}$

This is an open access article published by the IET under the Creative Commons Attribution License (http://creativecommons.org/licenses/by/3.0/)

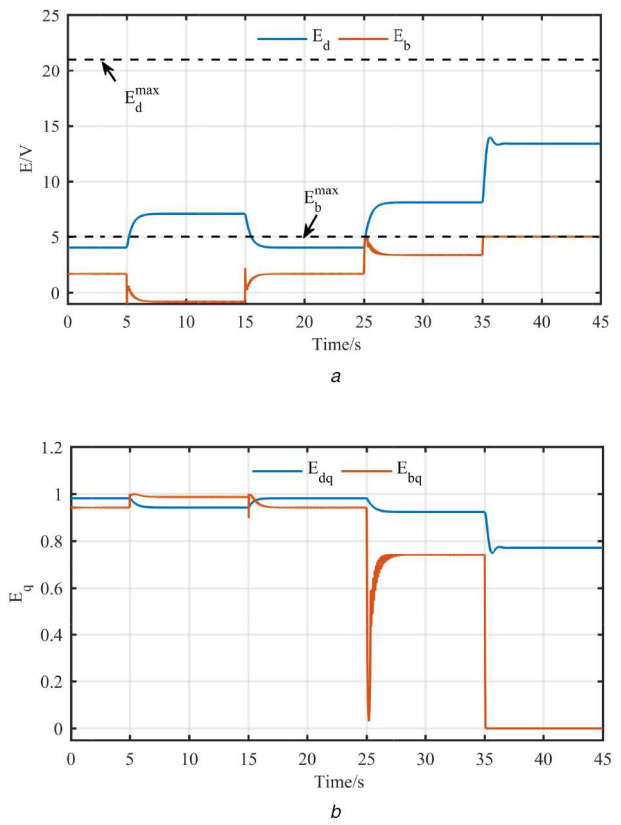

Fig. 8 *Dynamic response of the control states*
(a) Virtual voltages, ***(b)*** Additional control states

Table 2 Controller and system parameters

Parameters	Values	Parameters	Values
U_1	36 V	U_2	24 V
R_1	2.4 Ω	R_2	3 Ω
$L_{1,2}$	0.3 mH	$C_{1,2}$	300 μF
d_1	0.2	d_2	0.4
$r_{v1,2}$	20 V	k	1000
c_1	873	c_2	655
$E_1^{\max}$	30 V	E_2^{max}	50 V

and r_v should satisfy $i_L^{\max} = E^{\max}/(r_v + r_{in})$ in order to reach the upper limit of the converter. Nevertheless, it is clear that by ignoring this resistance, the current still remains below $i_L^{\max}$ as desired.

8 Conclusions

In this paper, a detailed control design was presented for multiple parallel operated three-phase AC/DC and bidirectional DC/DC boost converters in a DC micro-grid framework, loaded by a CPL. The nonlinear dynamic control scheme was developed to ensure load power sharing and output voltage regulation, with an inherent input current limitation. The stability of the entire DC micro-grid was analytically proven when the system supplies a CPL using singular perturbation theory. Introducing a constant virtual resistance with a bounded dynamic virtual voltage for the three-phase AC/DC and for the bidirectional DC/DC boost converter, it has been shown that the input currents of each converter will never violate a maximum given value. This feature is guaranteed without any knowledge of the system parameters and without any extra measures such as limiters or saturators, thus, addressing the issue of integrator wind-up and instability problems that can occur with the traditional overcurrent controllers' design. The effectiveness of the proposed scheme and its overcurrent capability are verified by simulating a DC micro-grid considering different load power

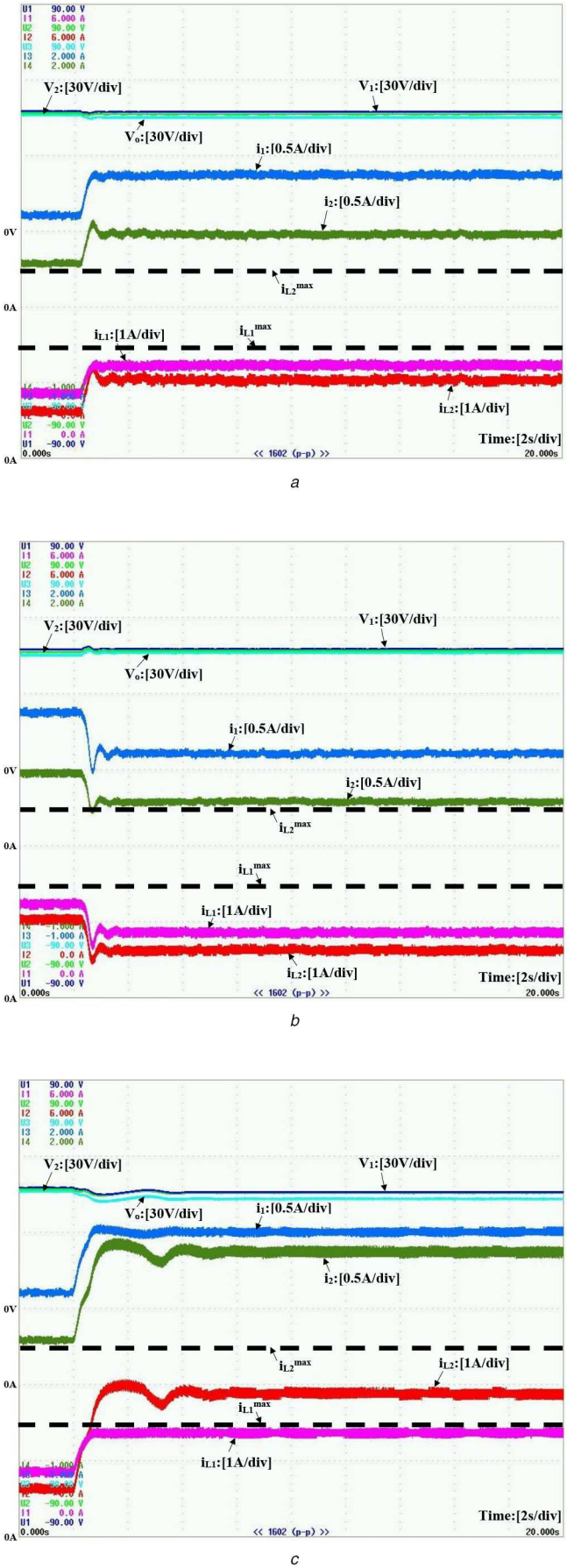

Fig. 9 *Experimental results under the proposed controller*
(a) Load demand increases from 40 to 60 W, ***(b)*** Load demand decreases from 60 to 40 W, ***(c)*** Load demand increases from 40 to 80 W

This is an open access article published by the IET under the Creative Commons Attribution License (http://creativecommons.org/licenses/by/3.0/)

variations and battery operations (charging, discharging), and by experimentally testing a parallel converter micro-grid configuration feeding an electronic load, acting as a CPL.

9 Acknowledgment

This work was supported by Engineering and Physical Sciences Research Council (EPSRC) under Grant EP/S001107/1 and Grant EP/S031863/1.

10 References

[1] Chen, Y., Chang, J.M.: 'EMAAS: cloud-based energy management service for distributed renewable energy integration', *IEEE Trans. Smart Grid*, 2015, **6**, (6), pp. 2816–2824

[2] Rahbar, K., Chai, C.C., Zhang, R.: 'Energy cooperation optimization in microgrids with renewable energy integration', *IEEE Trans. Smart Grid*, 2018, **9**, (2), pp. 1482–1493

[3] Luo, C., Huang, Y., Gupta, V.: 'Stochastic dynamic pricing for EV charging stations with renewable integration and energy storage', *IEEE Trans. Smart Grid*, 2018, **9**, (2), pp. 1494–1505

[4] Ma, Z., Pesaran, A., Gevorgian, V.*, et al.*: 'Energy storage, renewable power generation, and the grid: NREL capabilities help to develop and test energy-storage technologies', *IEEE Electrific. Mag.*, 2015, **3**, (3), pp. 30–40

[5] Mahmoodi, M., Gharehpetian, G.B., Abedi, M.*, et al.*: 'Control systems for independent operation of parallel DG units in DC distribution systems'. 2006 IEEE Int. Power and Energy Conf., Putra Jaya, Malaysia, 2006, pp. 220–224

[6] Schonberger, J., Duke, R., Round, S.D.: 'DC-bus signaling: a distributed control strategy for a hybrid renewable nanogrid', *IEEE Trans. Ind. Electron.*, 2006, **53**, (5), pp. 1453–1460

[7] Lu, X., Guerrero, J.M., Sun, K.*, et al.*: 'An improved droop control method for DC microgrids based on low bandwidth communication with DC bus voltage restoration and enhanced current sharing accuracy', *IEEE Trans. Power Electron.*, 2014, **29**, (4), pp. 1800–1812

[8] Huang, P.H., Liu, P.C., Xiao, W.*, et al.*: 'A novel droop-based average voltage sharing control strategy for DC microgrids', *IEEE Trans. Smart Grid*, 2015, **6**, (3), pp. 1096–1106

[9] Rasoolzadeh, A., Salmasi, F.R.: 'Reduced-order dynamic model for droop-controlled inverter/converter-based low-voltage hybrid AC/DC microgrids – part 2: DC sub-microgrid and power exchange', *IET Smart Grid*, 2018, **1**, (4), pp. 134–142

[10] Zhong, Q.C.: 'Robust droop controller for accurate proportional load sharing among inverters operated in parallel', *IEEE Trans. Ind. Electron.*, 2013, **60**, (4), pp. 1281–1290

[11] Shuai, Z., He, D., Fang, J.*, et al.*: 'Robust droop control of DC distribution networks', *IET Renew. Power Gener.*, 2016, **10**, (6), pp. 807–814

[12] Cingoz, F., Elrayyah, A., Sozer, Y.: 'Plug-and-play nonlinear droop construction scheme to optimize islanded microgrid operations', *IEEE Trans. Power Electron.*, 2017, **32**, (4), pp. 2743–2756

[13] Simpson-Porco, J.W., Dörfler, F., Bullo, F.: 'Voltage stabilization in microgrids via quadratic droop control', *IEEE Trans. Autom. Control*, 2017, **62**, (3), pp. 1239–1253

[14] Liu, X.Y., Forsyth, A.J.: 'Comparative study of stabilizing controllers for brushless DC motor drive systems'. IEEE Int. Conf. on Electric Machines and Drives, San Antonio, Texas, USA., 2005, pp. 1725–1731

[15] Mohamed, Y.A.I., Radwan, A.A.A., Lee, T.K.: 'Decoupled reference-voltage-based active DC-link stabilization for pmsm drives with tight-speed regulation', *IEEE Trans. Ind. Electron.*, 2012, **59**, (12), pp. 4523–4536

[16] Emadi, A., Khaligh, A., Rivetta, C.H.*, et al.*: 'Constant power loads and negative impedance instability in automotive systems: definition, modeling, stability, and control of power electronic converters and motor drives', *IEEE Trans. Veh. Technol.*, 2006, **55**, (4), pp. 1112–1125

[17] Rahimi, A.M., Emadi, A.: 'Active damping in DC/DC power electronic converters: A novel method to overcome the problems of constant power loads', *IEEE Trans. Ind. Electron.*, 2009, **56**, (5), pp. 1428–1439

[18] Cespedes, M., Xing, L., Sun, J.: 'Constant-power load system stabilization by passive damping', *IEEE Trans. Power Electron.*, 2011, **26**, (7), pp. 1832–1836

[19] Anun, M., Ordonez, M., Zurbriggen, I.G.*, et al.*: 'Circular switching surface technique: high-performance constant power load stabilization for electric vehicle systems', *IEEE Trans. Power Electron.*, 2015, **30**, (8), pp. 4560–4572

[20] Su, M., Liu, Z., Sun, Y.*, et al.*: 'Stability analysis and stabilization methods of DC microgrid with multiple parallel-connected DC-DC converters loaded by CPLs', *IEEE Trans. Smart Grid*, 2018, **9**, (1), pp. 132–142

[21] Middlebrook, R.D.: 'Input filter considerations in design and application of switching regulators'. Proc IEEE Industry Applications Annual Meeting, Chicago, IL, USA, 1976

[22] Wildrick, C.M., Lee, F.C., Cho, B.H.*, et al.*: 'A method of defining the load impedance specification for a stable distributed power system', *IEEE Trans. Power Electron.*, 1995, **10**, (3), pp. 280–285

[23] Liu, J., Feng, X., Lee, F.C.*, et al.*: 'Stability margin monitoring for DC distributed power systems via perturbation approaches', *IEEE Trans. Power Electron.*, 2003, **18**, (6), pp. 1254–1261

[24] Anand, S., Fernandes, B.G.: 'Reduced-order model and stability analysis of low-voltage DC microgrid', *IEEE Trans. Ind. Electron.*, 2013, **60**, (11), pp. 5040–5049

[25] Tahim, A.P.N., Pagano, D.J., Lenz, E.*, et al.*: 'Modeling and stability analysis of islanded DC microgrids under droop control', *IEEE Trans. Power Electron.*, 2015, **30**, (8), pp. 4597–4607

[26] Cucuzzella, M., Kosaraju, K.C., Scherpen, J.M.A.: 'Distributed passivity-based control of dc microgrids'. 2019 American Control Conf. (ACC), Philadelphia, PA, USA., 2019, pp. 652–657

[27] Namazi, M.M., Nejad, S.M.S., Tabesh, A.*, et al.*: 'Passivity-based control of switched reluctance-based wind system supplying constant power load', *IEEE Trans. Ind. Electron.*, 2018, **65**, (12), pp. 9550–9560

[28] Hassan, M.A., Li, E., Li, X.*, et al.*: 'Adaptive passivity-based control of DC–DC buck power converter with constant power load in DC microgrid systems', *IEEE J. Emerging Sel. Topics Power Electron.*, 2019, **7**, (3), pp. 2029–2040

[29] Zeng, J., Zhang, Z., Qiao, W.: 'An interconnection and damping assignment passivity-based controller for a dc–dc boost converter with a constant power load', *IEEE Trans. Ind. Appl.*, 2014, **50**, (4), pp. 2314–2322

[30] Zhong, Q.C., Konstantopoulos, G.C.: 'Nonlinear current-limiting control for grid-tied inverters'. 2016 American Control Conf. (ACC), Boston, MA, USA, 2016, pp. 7472–7477

[31] Konstantopoulos, G.C., Zhong, Q.: 'Current-limiting DC/DC power converters', *IEEE Trans. Control Syst. Technol.*, 2019, **27**, (2), pp. 855–863

[32] Bayati, N., Hajizadeh, A., Soltani, M.: 'Protection in DC microgrids: a comparative review', *IET Smart Grid*, 2018, **1**, (3), pp. 66–75

[33] Shen, Z.J.: 'Ultrafast solid-state circuit breakers: protecting converter-based AC and DC microgrids against short circuit faults', *IEEE Electrific. Mag*, 2016, **4**, (2), pp. 72–70

[34] Duan, F., Xu, M., Yang, X.*, et al.*: 'Canonical model and design methodology for LLC DC/DC converter with constant current operation capability under shorted load', *IEEE Trans. Power Electron.*, 2016, **31**, (10), pp. 6870–6883

[35] Li, Y., Mao, X., Wang, H.*, et al.*: 'An improved hiccup mode short-circuit protection technique with effective overshoot suppression for DC-DC converters', *IEEE Trans. Power Electron.*, 2013, **28**, (2), pp. 877–885

[36] Li, Y., Lai, X., Ye, Q.*, et al.*: 'Novel short-circuit protection technique for DC-DC buck converters', *IET Circuits Devices Syst.*, 2014, **8**, (2), pp. 90–99

[37] Tilli, A., Conficoni, C.: 'Control of shunt active filters with actuation and current limits', *IEEE Trans. Control Syst. Technol.*, 2016, **24**, (2), pp. 644–653

[38] Bottrell, N., Green, T.C.: 'Comparison of current-limiting strategies during fault ride-through of inverters to prevent latch-up and wind-up', *IEEE Trans. Power Electron.*, 2014, **29**, (7), pp. 3786–3797

[39] Zhong, Q.C., Konstantopoulos, G.C.: 'Current-limiting three-phase rectifiers', *IEEE Trans. Ind. Electron.*, 2018, **65**, (2), pp. 957–967

[40] Braitor, A., Baldivieso-Monasterios, P.R., Konstantopoulos, G.C.*, et al.*: 'Current-limiting droop control design of paralleled AC/DC and DC/DC converters in dc micro-grids'. IECON 2018 – 44th Annual Conf. of the IEEE Industrial Electronics Society, Washington DC, USA., 2018, pp. 132–137

[41] Lee, T.S.: 'Lagrangian modeling and passivity-based control of three-phase AC/DC voltage-source converters', *IEEE Trans. Ind. Electron.*, 2004, **51**, (4), pp. 892–902

[42] Ortega, R., Loria, A., Nicklasson, P.J.*, et al.*: '*Passivity-based control of euler-lagrange systems, mechanical, electrical and electromechanical applications*' (Springer-Verlag, Great Britain, 1998)

[43] Konstantopoulos, G.C., Zhong, Q.C., Ren, B.*, et al.*: 'Bounded integral control of input-to-state practically stable nonlinear systems to guarantee closed-loop stability', *IEEE Trans. Autom. Control*, 2016, **61**, (12), pp. 4196–4202

[44] Khalil, H.K.: '*Nonlinear systems*' (Pearson, USA., 2014, 3rd edn.)

This is an open access article published by the IET under the Creative Commons Attribution License (http://creativecommons.org/licenses/by/3.0/)